Arabidopsis TSO1 and MYB3R1 form a regulatory module to coordinate cell proliferation with differentiation in shoot and root

Wanpeng Wang[a,b], Paja Sijacic[a,1], Pengbo Xu[c], Hongli Lian[c], and Zhongchi Liu[a,2]

[a]Department of Cell Biology and Molecular Genetics, University of Maryland, College Park, MD 20742; [b]Plant Science Graduate Program, University of Maryland, College Park, MD 20742; and [c]School of Agriculture and Biology, Shanghai Jiaotong University, Shanghai 200240, China

Edited by Xuemei Chen, University of California, Riverside, CA, and approved February 20, 2018 (received for review September 9, 2017)

Fundamental to plant and animal development is the regulated balance between cell proliferation and differentiation, a process intimately tied to cell cycle regulation. In *Arabidopsis*, mutations in TSO1, whose animal homolog is LIN54, resulted in severe developmental abnormalities both in shoot and root, including shoot meristem fasciation and reduced root meristematic zone. The molecular mechanism that could explain the *tso1* mutant phenotype is absent. Through a genetic screen, we identified 32 suppressors that map to the *MYB3R1* gene, encoding a conserved cell cycle regulator. Further analysis indicates that TSO1 transcriptionally represses *MYB3R1*, and the ectopic MYB3R1 activity mediates the *tso1* mutant phenotype. Since animal homologs of TSO1 and MYB3R1 are components of a cell cycle regulatory complex, the DREAM complex, we tested and showed that TSO1 and MYB3R1 coimmunoprecipitated in tobacco leaf cells. Our work reveals a conserved cell cycle regulatory module, consisting of TSO1 and MYB3R1, for proper plant development.

MYB3R1 | DREAM complex | cell cycle | meristem | TSO1

An important distinction between animal and plant development is that the animal cell lineage is already determined during embryogenesis, while plant cells continuously develop and commit to new organs during postembryonic development, owing to the self-renewing stem cells at the two growing tips, the shoot apical meristem (SAM), and the root apical meristem (RAM). In addition, plant cells are highly plastic, capable of acquiring new cell identity in response to positional cues or environmental conditions. Despite the distinctions, plants and animals share conserved cell cycle regulatory machineries such as the cyclin–cyclin-dependent kinases (CDKs) and the DREAM complex (1–4). While tremendous insights into the cell cycle regulation were obtained from single cell studies such as yeast and mammalian cell culture (5, 6), the understanding of how the basic cell cycle machinery is integrated into the specific developmental context in animals and plants is lacking.

In *Arabidopsis*, the SAM consists of three periclinal cell layers (L1–L3) and is divided into the central zone (CZ), the peripheral zone (PZ) flanking CZ, and the rib zone (RZ) beneath the CZ. Slowly dividing stem cells are situated in the CZ and are promoted by the homeodomain transcription factor WUCHEL (WUS). Cells in the PZs give rise to leaf or flower primordia through rapid cell division (7). At the opposite pole, the RAM is organized distinctly from the SAM. The slow-dividing cells at the center of the root tip forms the quiescent center (QC), which is surrounded by initials that give rise to different root cell types. Arranged radially from the center to the peripheral of the root is the stele (vasculature and pericycle tissue), endodermis, cortex, epidermis, lateral root cap, and columella (8). The WUSCHEL-Related Homeobox 5 (*WOX5*) is expressed in the QC and maintains stem cell identity of the root initials (9). In the longitudinal axis of the root, cells near the root tip divide rapidly in the meristematic zone (MZ), then exit the mitotic cycle and enter the endocycle in the transition zone (TZ), and subsequently differentiate in the elongation zone (EZ).

Proper meristem organization and function relies heavily on proper cell cycle regulation. While slowly dividing cells such as stem cells must maintain themselves at the G1 or S phase for a long period of time, rapidly dividing cells like cells in emerging organ primordia must overcome cell cycle checkpoints in rapid successive cycles. Further, differentiating cells need to exit cell cycle permanently. Failure to maintain proper cell cycle regulation has devastating consequences. Retinoblastoma (*RB*), the first tumor suppressor gene found in animals, is a cell cycle regulator (10). Loss of the RB function in animals led to embryonic lethality and tumor (11, 12). Loss of the *RB-Related* (*RBR*) gene in *Arabidopsis* is gametophyte lethal (13–15). Conditional RNAi knockdown of *RBR* disrupts the stem cell maintenance and organ primordia initiation in the SAM (16). Investigations into how cell cycle regulation interacts with development will not only bring novel insights into the distinct developmental programs such as the SAM and RAM in higher plant development but will also uncover the conserved principles that balance cell proliferation with differentiation. This proper balance is critical to successful organogenesis and the prevention of undesirable growth such as tumor.

Central to this study is the *Arabidopsis tso1* mutant with defects in the SAM and RAM (17). The *tso1* mutant SAM has disorganized cell layers, enlarged cells with incompletely formed cell walls, and enlarged (fasciated) SAM. This is accompanied by failure to form floral organs, leading to complete sterility. These phenotypes suggest that loss of TSO1 activity leads to overproliferation of cells residing in the shoot apical meristem and failure in floral organ differentiation, indicating a role of *TSO1* in balancing cell proliferation with differentiation. The TSO1 protein

Significance

Plant postembryonic development relies on a small pool of stem cells at the shoot and root tip. The question of how the cell cycle regulatory activities are integrated into the specific stem cell context is not well understood. This study identifies a previously unknown regulatory module in the flowering plant consisting of two regulatory genes, *TSO1* and *MYB3R1*. TSO1 negatively regulates *MYB3R1* to control cell division activity, maintain proper stem cell pool size, and balance cell proliferation with differentiation in shoot and root. Significantly, animal homologs of TSO1 and MYB3R1 are members of a cell cycle regulatory complex, suggesting that this conserved module operates in both plants and animals.

Author contributions: W.W., P.S., and Z.L. designed research; W.W., P.S., P.X., and H.L. performed research; W.W. and Z.L. analyzed data; and W.W. and Z.L. wrote the paper.

The authors declare no conflict of interest.

This article is a PNAS Direct Submission.

[1]Present address: Department of Biology, Emory University, Atlanta, GA 30322.

[2]To whom correspondence should be addressed. Email: zliu@umd.edu.

This article contains supporting information online at www.pnas.org/lookup/suppl/doi:10.1073/pnas.1715903115/-/DCSupplemental.

Published online March 13, 2018.

possesses two cysteine-rich (CXC) domains connected by a conserved hinge domain (18, 19). It is homologous to the animal LIN54, a core subunit of an evolutionarily conserved cell cycle complex found in *Caenorhabditis elegans*, *Drosophila*, and mammals (20–26). This multisubunit complex functions as a master coordinator of cell cycle transcription (3). Since the sequence similarity between TSO1 and LIN54 is limited only to the DNA-binding CXC-hinge-CXC domain, whether *TSO1* plays a similar function in plants is not known.

Interestingly, two types of *tso1* mutant alleles gave two distinct developmental phenotypes. The *tso1-1* and *tso1-2* mutations (type I), which alter one of the conserved cysteines in the CXC domain, caused strong and multiple mutant phenotypes ranging from meristem fasciation to complete sterility (17). In contrast, type II alleles such as *tso1-3* to *tso1-6* were caused by nonsense mutation or T-DNA insertion and only showed reduced fertility (19, 27). The strong *tso1-1* mutation was shown to be recessive antimorphic as artificial miRNA targeting the mutant *tso1-1* mRNA significantly reduced the phenotype severity. Further, the type II *tso1-3* allele, when combined with a mutation in *SOL2*, *TSO1*'s closest paralog in *Arabidopsis*, showed a phenotype resembling *tso1-1*. Thus, *tso1-1* is equivalent to the combined loss of both *TSO1* and its paralog *SOL2* (28).

In *Arabidopsis*, there are seven paralogs of TSO1, which are classified into two subtypes based on distinct motifs found outside the CXC-hinge-CXC domain. Type I consists of *TSO1*/*At3G22780* and *SOL1*/*At3g22760* (*TCX3*), *SOL2*/*At4g14700* (*TCX2*), and *At3g04850* (*TCX4*). Type II consists of four other members, *At4g29000* (*TCX5*), *At2g20110* (*TCX6*), *At5g25790* (*TCX7*), and *At3g16160* (27). With the exception of *TSO1* and *SOL2*, there was no report of mutant phenotype associated with other family members. Interestingly, Kobayashi et al. (2) recently reported the isolation of two distinct plant DREAM complexes from *Arabidopsis* seedlings (4). The repressor complex acts in nonactively dividing cells to repress the cell cycle gene expression; it consists of ALY2/3, TCX5, RBR1, and repressors, E2FC and MYB3R3. The activator complex acts at the G2/M phase and consists of ALY3, TCX5, RBR1, DPA/B, and activators E2FB and MYB3R4 (2, 4). Both plant complexes contain TCX5, one of the TSO1 family members. The isolation of the DREAM complexes in *Arabidopsis* paved the way for further studies of how this conserved cell cycle complex acts in the context of plant development, for which little is understood.

To understand the mechanism of *TSO1* function in the SAM and RAM, we conducted a genetic screen to isolate genetic modifiers of *tso1-1*. We hypothesized that if *TSO1* acts in a plant DREAM complex, genes coding for the DREAM complex components or genes normally regulated by the complex could be identified as suppressors or enhancers of *tso1-1*. The identification of these genetic interactors should provide mechanistic insights into how TSO1 regulates the development of SAM and RAM. Among the 45 suppressors of *tso1-1* identified in this study, 32 are mutations in the *MYB3R1* gene, coding for an R1R2R3-MYB transcription factor (TF) homologous to the mammalian B-MYB (also called MYBL2). B-MYB is a known DREAM complex cofactor in animals (6, 20, 21). We showed that MYB3R1 is both a target of TSO1 and possibly a partner of TSO1. Loss-of-function mutations in the *MYB3R1* gene suppressed all aspects of *tso1-1* phenotype, strongly suggesting the existence of a TSO1-MYB3R1 regulatory module that operates in both the SAM and RAM to regulate proper shoot and root development. The study identifies a TSO1-MYB3R1 regulatory module, uncovers the module's specific function during the development of the SAM and RAM, and indicates the evolutionary conservation of DREAM complex components in balancing cell proliferation with differentiation in higher eukaryotes.

Results

Identification of *tso1-1* Suppressors. To determine the mechanism of *TSO1* function, we conducted a mutagenesis screen to identify critical coregulators or downstream targets of TSO1. The genetic interactors may help place *TSO1* into existing or novel regulatory pathways. *tso1-1* allele was chosen for the mutagenesis as *tso1-1* is 100% sterile, making fertility rescue easily identifiable.

Since *tso1-1* plants produce no seed, we developed an inducible system to conditionally rescue *tso1-1* to obtain *tso1-1* homozygous seeds for mutagenesis. TSO1 full-length cDNA fused with the rat glucocorticoid receptor (GR) hormone binding domain was driven by the constitutive *35S* promoter. The transgenic *tso1-1* plants (*tso1-1; 35S::TSO1-GR*) produced seeds upon treatment with dexamethasone (DEX) (Fig. 1 *B* and *C*). These seeds were then mutagenized with EMS. By screening the M2 progeny of about 3,000 M1 *tso1-1; 35S::TSO1-GR* plants, 45 suppressors were identified based on their ability to develop elongated siliques in the absence of DEX treatment (*SI Appendix*, Fig. S1*A*). The degree of suppression ranges from weak to strong based on the length of the siliques (Fig. 1 *D* and *E*) and the number of seeds in each silique (*SI Appendix*, Fig. S2).

The Majority of Suppressors Map to the *MYB3R1* Gene. To determine the molecular identity of these suppressors, we used the bulk-segregant mapping-by-sequencing approach. Five suppressors were crossed with the *tso1-1; 35S::TSO1-GR* parental line to yield F2 mapping populations (*SI Appendix*, Fig. S1*B*). For each suppressor line, genomic DNA samples from 35–50 F2 plants showing the suppressed phenotype were pooled and sequenced.

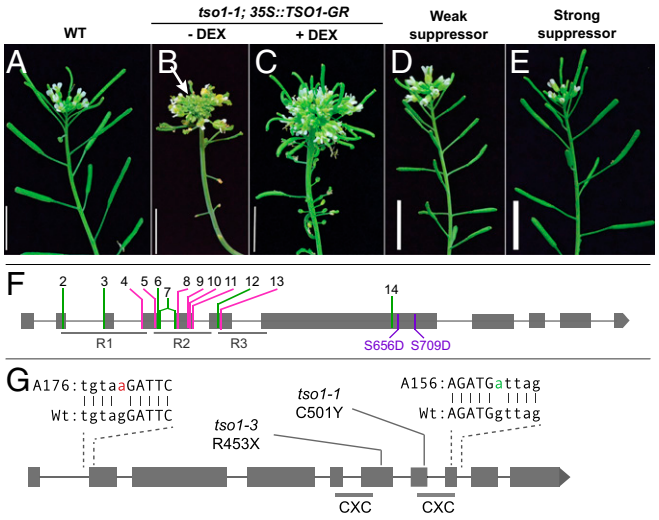

Fig. 1. *tso1-1* mutant phenotype and *tso1-1* suppressors. (*A*) Wild-type (WT/Ler) inflorescence showing elongated siliques and flowers at the apex. (*B*) The inflorescence shoot of a *tso1-1* mutant containing the *35S::TSO1-GR* construct. No dexamethasone (DEX) was applied and a lack of siliques is evident. An enlarged shoot apex (arrow) indicates meristem fasciation. (*C*) DEX treatment (+DEX) of *tso1-1* plants harboring the *35S::TSO1-GR* transgene resulted in the rescue of the fertility defect as shown by the formation of long siliques. The inflorescence fasciation was not rescued due to the late stage of DEX application. (*D*) The inflorescence shoot of a weak suppressor of *tso1-1*, showing short siliques. Although the suppressor plant contains the *35S::TSO1-GR*, no DEX was applied. (*E*) The inflorescence of a strong suppressor of *tso1-1*, showing normal size siliques. No DEX was applied. (*F*) Summary of *myb3r1* mutations and their locations within the *MYB3R1* gene. R1, R2, and R3 are the three DNA-binding domains. New *myb3r1* alleles identified by the suppressors are respectively named *myb3r1-2–myb3r1-14* (*SI Appendix*, Table S1). Nonsense or splicing mutations are labeled in green and missense mutations are labeled in pink. Serine 656 and serine 709 are changed into aspartic acid in the phosphomimic study. (*G*) Location of *tso1-1*, *tso1-3*, and the two intragenic suppressors *tso1-7* (A156) and *tso1-8* (A176). The exon sequence is in uppercase and the intron sequence is in lowercase. Specific changes in *tso1-7* and *tso1-8* are in magenta and green, respectively. The two CXC domains are underlined.

An analysis pipeline (*Materials and Methods*) mapped three suppressors (*A317*, *B636*, and *B763*) to the same region of chromosome 4 (*SI Appendix*, Fig. S3). Closer examination of the region revealed that the three suppressors caused either nonsense mutations (*A317* and *B763*) or missense mutation (*B636*) in the same gene *MYB3R1*/*At4G32730*, and they were subsequently named *myb3r1-14*, *-12*, and *-9*, respectively (Fig. 1*F* and *SI Appendix*, Table S1).

To determine whether any of the remaining suppressors also reside in *MYB3R1*, we performed complementation tests through pairwise crosses among the suppressors. The results showed that 29 of the 40 suppressors failed to complement *myb3r1* and hence defined additional alleles of *myb3r1* (Fig. 1*F* and *SI Appendix*, Table S1). Sequence analysis of 22 such new *myb3r1* suppressors identified specific mutational changes (*SI Appendix*, Table S1). Three alleles, *myb3r1-3*, *myb3r1-4*, and *myb3r1-14*, were isolated independently multiple times (*SI Appendix*, Table S1), suggesting saturation of the screen. In total, 13 independent new alleles (*myb3r1-2*–*myb3r1-14*) were confirmed (Fig. 1*F* and *SI Appendix*, Table S1). Seven are missense mutations, four are nonsense mutations, and two are splicing mutations. Twelve of the 13 alleles caused changes in the R1, R2, and R3 DNA-binding domains, indicating the essential function of the DNA-binding domains. Our data uncover *myb3r1* as the major suppressor of *tso1-1*.

The second locus identified by the *tso1-1* suppressors was *TSO1* itself. Two suppressors (*A156*/*tso1-7* and *A176*/*tso1-8*) were mapped to the same region of chromosome 3 (*SI Appendix*, Fig. S3) and each caused a mutation that affects the splicing of *TSO1* mRNA (Fig. 1*G* and *SI Appendix*, Table S1). A third *tso1* allele (*B378*/*tso1-9*) was identified among the remaining suppressors by complementation tests. The identification of intragenic *tso1-1* suppressors confirms our previous studies, indicating that *tso1-1* is a recessive antimorphic allele (28).

CRISPR-Induced *myb3r1* Mutations Suppress *tso1-1*. The EMS mutagen induced background mutations in the genome. Further, *myb3r1* mutations could potentially suppress *tso1-1* indirectly by facilitating TSO1-GR's entry into the nucleus in the absence of DEX treatment. To eliminate these possibilities, we used CRISPR/Cas9 to knockout *MYB3R1* directly in the *tso1-1* background (without the TSO1-GR transgene). A gRNA targeting the fourth exon of *MYB3R1* together with the *Cas9* construct was transformed into plants heterozygous for *tso1-1*. In T2 generation, several *tso1-1* mutant plants showed wild-type (WT) inflorescence branches and fertile siliques (Fig. 2*B*). These genetic mosaic plants contained CRISPR-induced biallelic mutations in the wild-type branches (Fig. 2*H*), indicating that the suppression of *tso1-1* by *myb3r1* is cell autonomous. Seeds collected from the wild-type branches gave rise to next generation plants that were indistinguishable from wild type (Fig. 2*C*). Therefore, germline-transmitted *myb3r1*^{CR} completely suppressed *tso1-1*. This experiment firmly established that *myb3r1* loss-of-function mutations suppress *tso1-1* and eliminated any potential complication due to the *TSO1-GR* transgene.

***myb3r1* Mutations Suppress Different *tso1* Alleles.** To determine whether *myb3r1* also suppresses the other type of *tso1* alleles, the same CRISPR/Cas9 construct was transformed into *tso1-3*, which harbors a nonsense mutation between the two CXC domains and shows reduced fertility (18, 28, 29) (Fig. 2*D*). In the *tso1-3* background, plants heterozygous for the *myb3r1*^{CR} mutation showed slightly elongated siliques compared with *tso1-3* single mutant plants (Fig. 2 *E* and *G*) due to the formation of about a quarter homozygous *myb3r1*^{CR} seeds. Further, *tso1-3* plants homozygous for *myb3r1*^{CR} are wild-type-like (Fig. 2 *F* and *G*). Therefore, *myb3r1* mutations suppress both *tso1-1* and *tso1-3*, and the effect of suppression is gene specific, not allele specific. The observation that *myb3r1* mutations suppressed all defects of *tso1* alleles indicates that *MYB3R1* participates in all developmental processes regulated by *TSO1*.

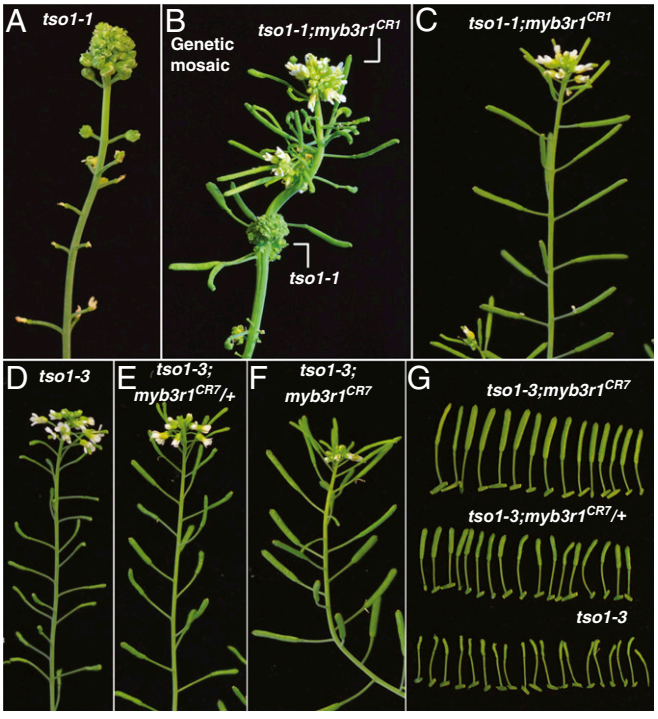

Fig. 2. CRISPR-edited *myb3r1* alleles suppress both *tso1-1* and *tso1-3*. (*A*) Inflorescence of *tso1-1* mutant. (*B*) A genetic mosaic *tso1-1* plant (T2 generation), which gives rise to wild-type branches with long siliques due to suppression of *tso1-1* by the CRISPR-edited *myb3r1*^{CR} allele. (*C*) T3 generation *tso1-1; myb3r1*^{CR} plant derived from seeds collected from the wild-type branches of the mosaic plant shown in *B*. (*D*) *tso1-3* plant showing severely reduced fertility; most seeds homozygous for *tso1-3* are defective, leading to very small siliques. (*E*) *tso1-3* plant heterozygous for a CRISPR-edited *myb3r1*^{CR7} allele. A total of 75% of seeds derived from the heterozygous mother should be normal, leading to increased seed yield and larger siliques. (*F*) *tso1-3* plant homozygous for the CRISPR-edited *myb3r1*^{CR7} allele. The *tso1-3; myb3r1*^{CR7} double mutant developed normal siliques. Plants in *D*–*F* are siblings. (*G*) Closeup of the siliques made by plants in *F* (*Upper*), *E* (*Middle*), and *D* (*Lower*). (*H*) Sequence of *MYB3R1* targeted by the gRNA and CRISPR-edited changes in the *tso1-1* or *tso1-3* background.

Mutations in *MYB3R4* Do Not Suppress *tso1*. *MYB3R1* is one of the five genes in *Arabidopsis* that encode homologs of the conserved cell cycle regulator B-MYB (MYBL2) in mammals (30–32). MYB3R1 and MYB3R4 were previously considered redundant MYB3Rs. While single *myb3r1* and *myb3r4* mutants had no phenotype, double *my3r1*; *myb3r4* mutants showed a defect in mitosis and a reduction of G2/M cell cycle gene expression in the leaf stomatal cells (33). We thus asked why *myb3r4* mutation was absent among the *tso1-1* suppressors. Is the *MYB3R4* region recalcitrant to the EMS mutagen? Or is *MYB3R4* not involved in *TSO1*-regulated processes? The CRISPR/Cas9 system was used to target the second exon of *MYB3R4* (Fig. 3*E*). *tso1-1; myb3r4*^{CR1} double homozygous mutants are indistinguishable from *tso1-1* single mutants (Fig. 3 *A* and *B*). Hence, the *my3r4* loss-of-function mutation did not suppress *tso1-1*.

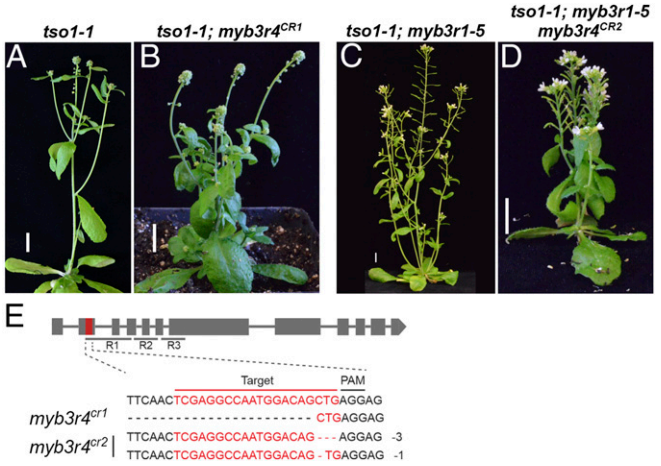

Fig. 3. *MYB3R4* is not part of the *TSO1-MYB3R1* module. (*A*) *tso1-1* plant. (*B*) *tso1-1; myb3r4*^{CR1} plant exhibiting the same phenotype as *tso1-1* single mutant. The specific mutations in *MYB3R4*^{CR1} are shown in *E*. (*C*) *tso1-1; myb3r1-5* plant with a mild phenotype (reduced fertility). (*D*) *tso1-1; myb3r1-5; myb3r4*^{CR2} plant showing a similar fertility defect (small siliques) as the plant in *C*. The specific biallelic sequence changes in *MYB3R4*^{CR2} are shown in *E*. (*E*) *MYB3R4* gene structure and CRISPR-edited mutations. R1R2R3 coding regions are underlined. The red sequence in the second exon of *MYB3R4* was targeted by the gRNA. (Scale bars in *A*–*D*, 1 cm.)

To test whether *MYB3R4* functions redundantly with *MYB3R1* in interacting with *tso1*, we tested whether *myb3r4*^{CR} could enhance the suppressor effect of *myb3r1-5*. *myb3r1-5* is a hypomorphic allele and a weak suppressor of *tso1-1* (Fig. 3 *A* and *C*). Compared with *tso1-1; myb3r1-5*, the triple mutant *tso1-1; myb3r1-5; myb3r4*^{CR2} did not appear to show any suppression of the fertility defect (Fig. 3 *C* and *D*). The smaller stature of the triple mutant was reminiscent of the *myb3r1-1; myb3r4-1* double mutant (33). Taken together, we concluded that *MYB3R1* and *MYB3R4* do not act redundantly with respect to the TSO1-regulated processes.

***MYB3R1* Is Misexpressed in *tso1-1* SAM.** To investigate the molecular mechanism underlying the observed genetic interaction between *tso1* and *myb3r1*, we examined *MYB3R1* gene expression in *tso1-1* mutants. A promoter *pMYB3R1*::*GUS* reporter construct published previously (31) was transformed into plants heterozygous for *tso1-1*. T1 transgenic plants heterozygous for *tso1-1* gave rise to both *tso1-1* and wild-type progeny, which were stained for 5-bromo-4-chloro-3-indolyl β-D-glucuronide (X-Gluc). The GUS expression pattern between *tso1-1* and its wild-type siblings was compared. Consistently across multiple transgenic lines, increased intensity as well as ectopic expression of GUS were observed in *tso1-1* inflorescences compared with their wild-type siblings (Fig. 4*A*). This reveals that the *MYB3R1* promoter activity is affected by *tso1-1*, and the ectopic expression and overexpression of *MYB3R1* likely mediate the *tso1-1* phenotype. The data suggest that TSO1 normally represses the transcription of *MYB3R1* in the SAM.

A translational fusion of *MYB3R1* to 3xeGFP using its native promoter (*gMYB3R1-NLS-3xeGFP*) was made to visualize MYB3R1 protein accumulation. In the wild-type SAM, nuclear GFP signal is observed in most cells with varying intensity (Fig. 4*B*). A small number of cells with brighter GFP signal are at the L1 and L2 layers of the emerging primordia (Fig. 4*B*, arrows). At the surface view of the inflorescence apex (Fig. 4*C*), the cells in emerging floral meristems and organ primordia showed brighter GFP signals and different GFP intensity in different cells, which suggests cell cycle regulated expression (34). In the *tso1-1* plant derived from the same transgenic line, the SAM longitudinal sections revealed the presence of larger cells with variable nuclei size and shape, and that the three-cell layer SAM organization was disrupted (17) (Fig. 4*B*). The *gMYB3R1-NSL-3xeGFP* signal appeared much brighter in *tso1-1* SAM, reflecting an increased MYB3R1 protein level in *tso1-1* (Fig. 4*B*).

A translational reporter of *TSO1* (fused to NLS-3xeGFP) was also made, utilizing a 4.1-kb *TSO1* genomic sequence including a 1-kb promoter and the *TSO1* coding region. Wild-type plants containing the *gTSO1-NLS-3xeGFP* construct showed nuclear GFP signal in the inflorescence meristem and floral meristem cells (Fig. 4 *D* and *E*). The sporadic expression pattern is reminiscent of genes under cell cycle regulation (34). This study indicates that *TSO1* and *MYB3R1* are both expressed in the SAM; they may cooperate with each other to regulate cell cycle genes, which may include themselves.

***myb3r1* Mutations also Suppress *tso1-1* Root Phenotype.** To determine whether *tso1-1* affects root development, we took advantage of the *TSO1-GR* inducible system to obtain *tso1-1* homozygous seeds. *tso1-1* seeds germinated on MS plates showed significantly reduced root length (Fig. 5*A*). In contrast, *tso1-3* did not exhibit this root defect (Fig. 5*A*). To investigate the underlying reason for the short root phenotype of *tso1-1*, we examined root cell organization using confocal microscopy. Roots were stained with propidium iodide (PI), and the root meristem size was measured by counting the number of cells in the cortex cell file in the MZ (Fig. 5*B*, the region between

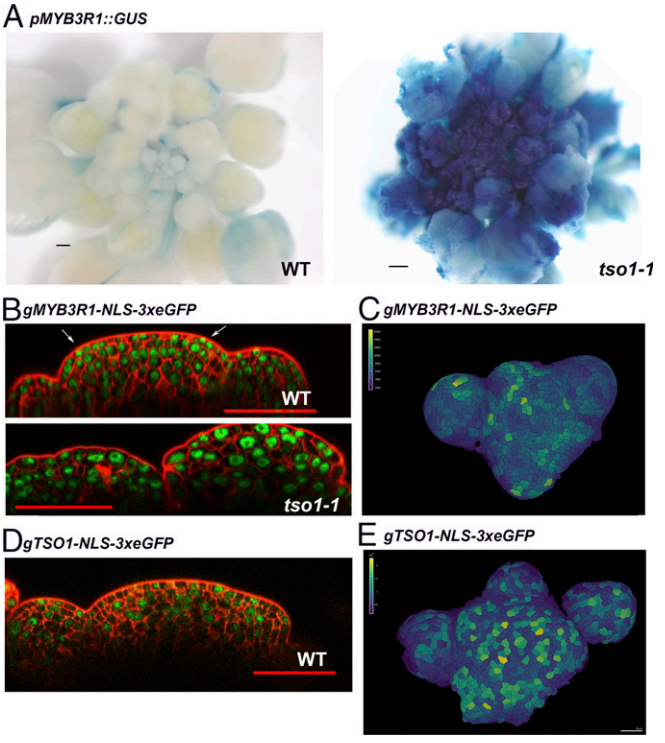

Fig. 4. *MYB3R1* is misexpressed in the *tso1-1* SAM. (*A*) *pMYB3R1::GUS* expression in wild-type (*Ler*) and in *tso1-1* inflorescence. The GUS signal is both ectopically expressed throughout the inflorescence and at a significantly higher level in *tso1-1*. The WT and *tso1-1* plants are siblings harboring the same *pMYB3R1::GUS* transgene and stained in X-Gluc for the same amount of time. (*B*) *gMYB3R1-NLS-3xeGFP* expression in wild-type (*Ler*) and *tso1-1* SAM. The WT and *tso1-1* plants are siblings harboring the same *gMYB3R1-NLS-3xeGFP* insertion. (*C*) Top-down view of a WT inflorescence meristem containing the *gMYB3R1-NLS-3xeGFP* transgene. GFP fluorescent signals inside 3D segmented cells were visualized as heat map. Fluorescent quantification of segmented cells provided quantitative signal. (*D*) *gTSO1-NLS-3xeGFP* expression in WT SAM. (*E*) Top-down view of a WT inflorescence meristem containing the *gTSO1-NLS-3xeGFP* transgene. GFP fluorescent signals inside the 3D segmented cells were visualized as heat map. [Scale bars, 200 μm (*A*), 50 μm (*B* and *D*), and 20 μm (*C* and *E*).]

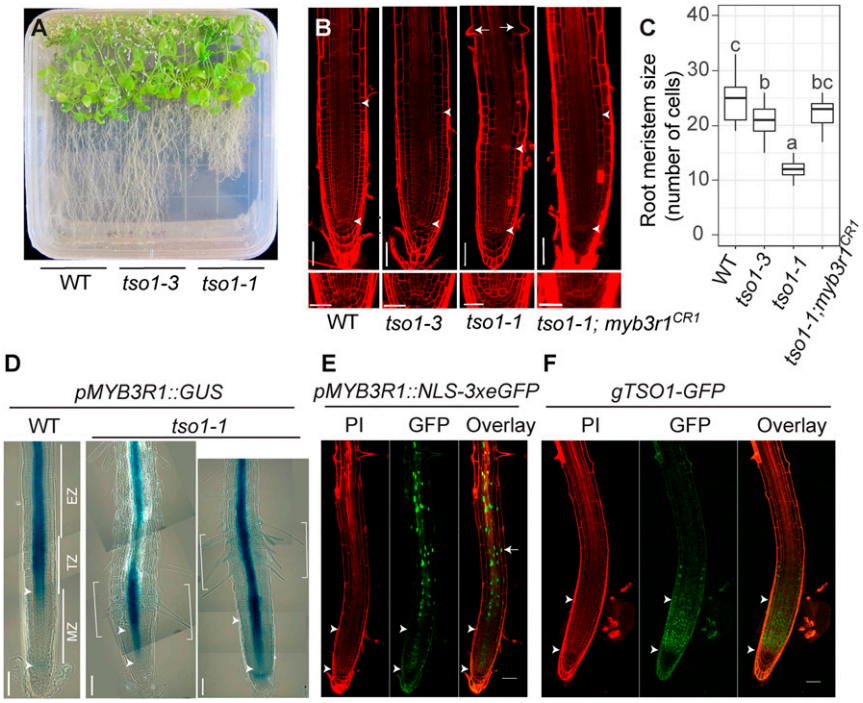

Fig. 5. The *tso1-1* short root phenotype is suppressed by *myb3r1* mutations. (*A*) WT (L*er*), *tso1-3*, and *tso1-1* seedlings on a half strength MS media plate at 42 d postgermination (dpg). (*B*) Confocal images of root apical meristem of WT (L*er*), *tso1-3*, *tso1-1*, and *tso1-1; myb3r1*^{CR1} at 7 dpg. The *Upper* arrowhead marks the upper boundary of the MZ as it marks the first cortex cell that is twice the size of the previous cell (cortex cell layer is the second from the epidermis). The *Lower* arrowhead marks the lower boundary of the MZ as well as the position of quiescent center (QC). Early differentiation of *tso1-1* root is indicated by precocious formation of root hairs (arrows). *Lower* shows the stem cell niche in the root of respective genotype. [Scale bars, 50 μm (*Upper*) and 25 μm (*Lower*).] (*C*) Quantification of root MZ size by the cell number in cortex file in MZ (n = 10–15 roots). Different letters indicate statistically significant difference ($P < 0.01$, one-way ANOVA and Tukey test). (*D*) *pMYB3R1::GUS* expression in wild-type and *tso1-1* root at 7 dpg. The MZ near the root tip is followed by the TZ, and then the EZ, which is shown by several images joined together with each image capturing a segment of the root. GUS signal, which reflects the promoter activity of *MYB3R1*, is restricted to the stele in the TZ and EZ. In *tso1-1* mutant, the bracketed segment showing strong GUS signal is shifted downward. The region of ectopic *MYB3R1* expression correlated with dense root hair formation. (*E*) In *pMYB3R1::NLS-3xeGFP* WT plant, nuclear GFP signals are found in the stele of the root in the EZ and the TZ, consistent with the GUS signal in *D*. (*F*) In WT plants containing the *gTSO1-GFP* construct, nuclear *TSO1-GFP* is largely restricted in the MZ and appears complementary to the *MYB3R1* expression zone. Propidium iodide (PI) staining gives the red outline of the root cells. [Scale bars, 50 μm (*B*, *E*, and *F*) and 100 μm (*D*).]

two arrowheads). The MZ was defined from the quiescent center to the first elongated cortex cell (35, 36). *tso1-1* roots had significantly reduced root meristematic zone (Fig. 5 *B* and *C*); precocious differentiation of the root epidermal cells was indicated by the precocious root hair formation (Fig. 5*B*). The *tso1-1* mutant root had all correct cell types with stereotypical division of the cortex/epidermal initials, and its QC did not terminate prematurely (Fig. 5*B*, *Lower*). Based on these results, we concluded that the short root phenotype of *tso1-1* was due to precocious transition from proliferation to differentiation.

Interestingly, the *tso1-1* root phenotype appears opposite that of the triple *myb3r1/3/5* mutant, whose root MZ is longer than wild type (2). This suggests that TSO1 and MYB3R1 may play opposite roles in regulating RAM, and that *TSO1* likely represses *MYB3R1* transcription in the root. To test this hypothesis, we examined the expression of the *pMYB3R1::GUS* transcriptional reporter in wild-type and *tso1-1* plants. In wild type, *pMYB3R1::GUS* showed a strong and specific expression in the vascular tissue spanning the EZ and TZ (Fig. 5*D*). The expression decreases precipitously upon entering the MZ (Fig. 5*D*). In *tso1-1* mutant root, the *pMYB3R1::GUS* expression extended further into the MZ. Furthermore, strong and precocious *pMYB3R1::GUS* expression (bracketed in Fig. 5*D*) often correlated with dense root hair formation. This *pMYB3R1::GUS* expression suggests that *TSO1* normally represses *MYB3R1* transcription in the MZ and that a loss of *TSO1* in *tso1-1* leads to ectopic *MYB3R1* transcripts in the MZ. Precocious root differentiation occurs as a result, which is indicated by the formation of root hairs and a reduced size of the MZ. In support of this, the *tso1-1; myb3r1*^{CR1} double mutation, which removes the ectopic *MYB3R1* in the *tso1-1* background, suppressed the short root phenotype of *tso1-1* (Fig. 5 *B* and *C*). Thus, ectopic/precocious *MYB3R1* activity in *tso1-1* mediates the short root phenotype.

The role of *TSO1* in repressing *MYB3R1* transcription in the root is consistent with the expression of *gTSO1-GFP* in the MZ (Fig. 5*F*) and the absence of (or low) *pMYB3R1-3xeGFP* transcription reporter signal in the MZ (Fig. 5*E*). In the TZ and EZ of the root, the reverse pattern was observed: the *pMYB3R1-3xeGFP* transcriptional reporter showed a strong GFP signal in the vascular tissue of TZ and EZ (Fig. 5*E*), where the *gTSO1-GFP* translational reporter had no signal (Fig. 5*F*). The MZ-specific expression of *TSO1* was consistent with the previous "root map" data (37), where *TSO1* transcripts were found in clusters 4 and 10 with the highest expression in the root MZ (*SI Appendix*, Fig. S4). Taken together, the complementary expression domains between *TSO1-GFP* protein and *MYB3R1* promoter reporter, the opposite root mutant phenotypes, and the genetic suppression of *tso1-1* by *myb3r1*^{CR} provided strong support for a negative regulatory relationship between these two genes. *TSO1* normally represses *MYB3R1* transcription in the root MZ to prevent *MYB3R1* expression and maintain meristematic activity. The data also suggest the existence of a TSO1-MYB3R1 regulatory module in the RAM as well as SAM.

Phosphomimics at S656 of MYB3R1 Enhances *tso1-3* Fertility Defect. To investigate whether the observed *tso1-1* phenotype is mediated

solely by misexpression of *MYB3R1* at the transcriptional level, we tested whether overexpression of *MYB3R1* could also cause the *tso1-1* mutant phenotype. *MYB3R1* cDNA was fused to the *35S* promoter and transformed into wild-type plants, but the resulting transgenic plants were wild type in phenotype (*SI Appendix*, Table S2 and Fig. S5*B*). The same *35S::MYB3R1* transgene also failed to enhance the weak *tso1-3* allele (*SI Appendix*, Table S2). Subsequently, we showed that the *35S::MYB3R1* construct failed to complement *myb3r1-9* when introduced into *tso1-1; myb3r1-9* plants (*SI Appendix*, Table S2 and Fig. S5 *C* and *D*). Hence, the 35S promoter could not be used to overexpress *MYB3R1*.

We then tested whether a hyperactive MYB3R1 could mediate a *tso1*-like phenotype. During late G1/S, mammalian B-MYB is phosphorylated by cyclin A/E-CDK2, which enhances its transactivation activity (38, 39). Therefore, we tested whether phosphomimics of MYB3R1 could lead to a *tso1*-like phenotype. By searching the *Arabidopsis* Protein Phosphorylation Site Database (PhosPhAt 4.0) (40, 41), serines at position 656 and 709 of MYB3R1 were found to be phosphorylated in previous large-scale phosphoproteomic studies (42, 43). Accordingly, we made a genomic construct of *MYB3R1* (*gMYB3R1*) containing the *MYB3R1* native promoter and coding sequence fused to GFP. The construct was shown to complement the *myb3r1-9* when introduced into *tso1-1; myb3r1-9* plants (*SI Appendix*, Table S2 and Fig. S5*E*). When introduced into WT or *tso1-3* background, the *gMYB3R1* construct had no phenotypic effect on the resulting plants (Fig. 6 *B* and *F*) even when the transgene is expressed at a high level (*SI Appendix*, Fig. S6*C*).

Subsequently, we modified this *gMYB3R1* by changing serine 656 and serine 709, respectively, into aspartic acid. These *gMYB3R1* (*S656D*) and *gMYB3R1* (*S709D*) "phosphomimic" constructs were respectively transformed into wild type and *tso1-3*. The *gMYB3R1* (*S709D*) phosphomimic had no phenotypic impact on the resulting transgenic plants (Fig. 6 *D* and *H*). In contrast, the *gMYB3R1* (*S656D*) transgene, while having no effect in the wild-type background (Fig. 6*C*), enhanced the *tso1-3* fertility defect (Fig. 6*G*). Three *tso1-3; gMYB3R1* (S656D) transgenic lines were analyzed further by quantifying their enhanced phenotype as well as the level of transgene expression (*SI Appendix*, Fig. S6). Line 8 had the lowest transgene expression and also the least enhancement of *tso1-3* among the three transgenic lines. However, none of these lines showed a defect in the SAM fasciation (Fig. 6*G* and *SI Appendix*, Fig. S6*A*, *Lower*). Together, these results suggest that serine 656 is an important regulatory site of MYB3R1 and that phosphorylation at serine 656 (but not serine 709) may promote MYB3R1 activity. Our data also indicate that increased/ectopic *MYB3R1* expression in *tso1-1* mutants or hyperactive MYB3R1 via posttranscriptional modification (such as S656D) are both able to cause *tso1*-like phenotypes.

MYB3R1 Coimmunoprecipitates with TSO1 in Tobacco Leaves. *TSO1* and *MYB3R1* both encode homologs of proteins that are components and cofactors of the animal and plant DREAM complex, thus we tested whether TSO1 and MYB3R1 associate with each other in a similar complex in plants. Since *TSO1* is expressed at a low level in *Arabidopsis*, we used a tobacco transient expression system, where *35S::YFP-MYB3R1* and *35S::Flag-TSO1* were transiently coexpressed in the tobacco leaves. Antibody against the Flag-epitope was used to pull down extracted plant proteins that were subsequently subjected to Western blots. Both Flag-tagged TSO1 and YFP-tagged MYB3R1 were detected in the Western blots (Fig. 7*A*), indicating that TSO1 physically interacts with MYB3R1. The reciprocal pulldown was also performed using anti-GFP antibody in the pulldown; both Flag-TSO1 and YFP-MYB3R1 were detected in the immunoprecipitated fraction by Western blots (Fig. 7*B*). This coimmunoprecipitation suggests the possibility of a DREAM-like complex that includes TSO1 and MYB3R1. Our work in previous sections demonstrated that TSO1 represses *MYB3R1* transcription; these co-IP data suggest that MYB3R1 may form a complex with TSO1 to participate in the regulation of its own transcription. The overlapping expression domains of the MYB3R1-GFP fusion protein and the TSO1-GFP fusion protein revealed by the *gMYB3R1-NLS-3xeGFP* and *gTSO1-NLS-3xeGFP* translational reporters in the SAM (Fig. 4 *B* and *D*) are consistent with this possibility.

Discussion

The Animal DREAM Complex and Its Likely Conserved Function in Plants. In the past 10–15 y, a new multiprotein complex, the DREAM complex, has gained increasing recognition as a critical cell cycle regulator. The DREAM complex not only coordinates G1/S with G2/M phases but also maintains cells at the G0 quiescent phase. Found in *Drosophila*, *C. elegans*, and mammals (22, 25, 26),

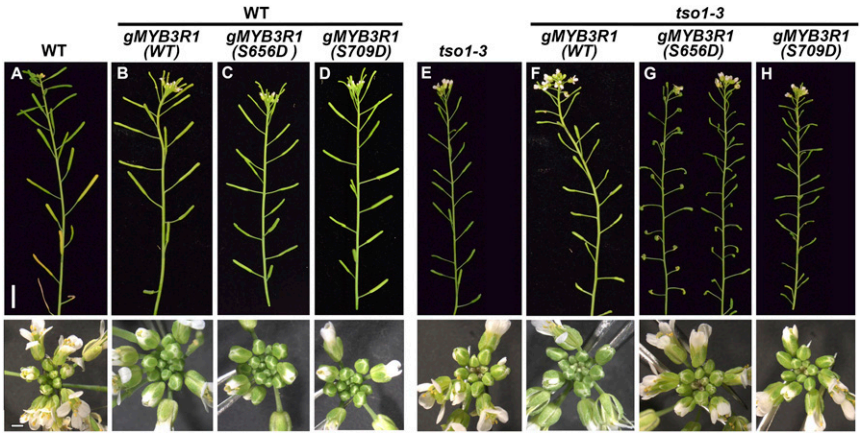

Fig. 6. *MYB3R1* phosphomimic S656D enhanced *tso1-3* mutant. (*A*) The main inflorescence of WT (L*er*). *Lower* shows the apex of the inflorescence. (*B–D*) Different versions of gMYB3R1 transgene constructs transformed into WT plants (genotype *tso1-1*/+). The specific version of transgene is indicated in parentheses. The main inflorescence shoot of *gMYB3R1* (*WT*) (*B*), *gMYB3R1* (*S656D*) (*C*), and *gMYB3R1* (*S709D*) (*D*) all showed wild-type phenotype. (*E*) The inflorescence of *tso1-3*. Note the small silique due to reduced fertility and the minor phyllotaxy defect. (*F–H*) Different versions of *gMYB3R1* transgene constructs transformed into *tso1-3* plants. (*F*) The main inflorescence shoot of *tso1-3; gMYB3R1* (*WT*) plant showing a phenotype that is identical to *tso1-3* single mutant. (*G*) The inflorescence shoots of two transgenic lines of *tso1-3; gMYB3R1* (*S656D*) plants showing a stronger phenotype than *tso1-3* single mutants. The siliques did not form properly due to abnormal gynoecium and severely reduced fertility. (*H*) The inflorescence of a *tso1-3; gMYB3R1* (*S709D*) plant. The phenotype is identical to that of *tso1-3*. [Scale bars, 1 cm (*Upper*) and 1 mm (*Lower*).]

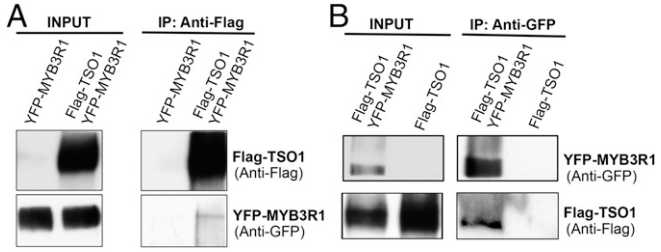

Fig. 7. TSO1 physically interacts with MYB3R1. Immunoprecipitation (IP) using protein extracts from tobacco leaves transiently expressing *35S::YFP-MYB3R1* and *35S::Flag-TSO1*. (*A*) Coimmunoprecipitation using anti-Flag antibody. YFP-MYB3R1 was detected in the pulldown by Western blots using the anti-GFP antibody. The tobacco leaves transiently expressing only *35S::YFP-MYB3R1* were used as a negative control. The experiments were performed twice with the same result. (*B*) Coimmunoprecipitation using anti-GFP antibody. Flag-TSO1 was detected in the pulldown by Western blots using the anti-Flag antibody. Tobacco leaves transiently expressing only *35S::Flag-TSO1* were used as a negative control.

the core complex of DREAM consists of five conserved members: LIN9, LIN37, LIN52, LIN54, and LIN53 (or RBBP4 in mammals). Depending on the organism, these components are also called MYB-interacting protein (MIP) or multivulva class B proteins (MuvB) (4). The core complex associates with different cofactors at different cell cycle phases. In G0 phase, the core complex binds to RB-like pocket proteins (p130 or p107) and repressor E2F/DP to repress all cell cycle-dependent gene expression. At the G1-to-S checkpoint, cyclin– CDKs phosphorylate RB-like pocket proteins to release E2F, which activates G1/S phase genes and promotes cell cycle progression. At the S phase, the DREAM core complex recruits MYB (B-MYB) and then recruits FOXM1 to the promoters of G2/M phase-expressed genes to promote their expression. Hence the core complex components support both repression and activation of gene expression and coordinate cell cycle phase-specific gene expression (3).

LIN54 (or mip120), the animal homolog of TSO1, is an essential core subunit of DREAM and confers DNA-binding activity to the DREAM complex (44). A predicted helix-coil-helix domain in LIN54 was required for its interaction with p130 and B-MYB. A reduction of LIN54 via RNAi disrupted the DREAM complex core, compromised the G1/S checkpoint, and downregulated G2/M cell cycle genes in human cell lines (44–46). In *Drosophila*, mutation in mip120 caused complex phenotypes, including shortened longevity and severe eye defect (21). Interestingly, the *Drosophila myb* mutant adult lethality can be suppressed by mutations in the DREAM core component mip130 (47), demonstrating that mutating the interdependent DREAM complex components can lead to almost normal phenotype, which is similarly demonstrated in our study.

Arabidopsis genome encodes homologs of almost all DREAM complex components (2), suggesting the possibility of a DREAM-like complex in plants. Indeed, at least two distinct DREAM complexes were recently isolated from seedling and leaves that consist of RBR1, E2Fs, MYB3R3, ALYs, and TCX5 (2). MYB3R1 and TSO1 are respective paralogs of MYB3R3 and TCX5 in *Arabidopsis*, suggesting the likely existence of analogous DREAM complexes consisting of TSO1 and MYB3R1 in shoot and root tissues. This hypothesis is supported by our co-IP data (Fig. 7) showing an association between TSO1 and MYB3R1. Interestingly, TSO1 does not possess the helix-coil-helix domain present in LIN54 and may interact with MYB3R1 via distinct domains or other binding partners. The striking mutant phenotypes shown by *tso1-1* and the complete suppression by *myb3r1* provide an unusual opportunity to study the plant DREAM-like complex function in higher plant development.

***Arabidopsis MYB3R1* Function and Regulation Bears Similarity to Mammalian B-MYB.** The mammalian B-MYB (MYBL2) resembles MYB3R1 in its cell cycle function and regulation (48). In G0/G1 cell cycle phase, *B-MYB* is repressed by the DREAM complex. In late G1/S, B-MYB is gradually released from the inhibition by the DREAM complex and instead associates with the core DREAM complex to cooperatively activate the G2/M cell cycle genes. Deregulation of B-MYB expression is involved in cancer initiation and progression; high B-MYB expression is correlated with poor patient outcome in numerous cancers (48, 49). The ectopic and extremely high level of *MYB3R1* expression in *tso1-1* mutant may cause what would be plant cancers: extreme meristem fasciation with many more meristem cells and failure of floral organ differentiation as shown in *tso1-1* mutants.

We showed that the CRISPR knockout of *MYB3R1* in *tso1-1* provided a highly effective and comprehensive suppression of abnormal *tso1-1* phenotypes. The *tso1-1* suppressor screen provided unprecedented information on the critical domains and residues of *MYB3R1*, which is highly relevant to the understanding of the domains and functions of B-MYB and its role in human cell cycle regulation and cancer initiation, prognosis, and treatment. Among the 13 new MYB3R1 alleles, 12 reside in the DNA-binding domain, demonstrating the significance of this conserved domain in the MYB protein function. *myb3r1-11* (C125Y), a strong suppressor of *tso1-1*, altered the conserved Cys125 residue in the R2 domain; Cys-125 was thought of as a redox sensor for the MYB protein (50) and an equivalent mutation in human MYB (Cys130) significantly impaired the activity of c-Myb and v-Myb (51, 52). Among the weak suppressors, *myb3r1-5* (G88R) resides in the loop region connecting R1 and R2 (Fig. 1*F*). *myb3r1-14* (R652X) causes a premature stop codon that removes the C-terminal region containing the serine 656. Alteration of this residue as demonstrated in the S656D phosphomimics has functional consequences. Future work will be necessary to test whether S656D might modulate TSO1-MYB3R1 protein–protein interaction, or constitutively activate downstream events, or both.

***MYB3R1* Is both an Activator and Repressor.** The *Arabidopsis* genome has about 130 MYB genes, the majority of which are in the R2R3-MYBs (MYB2Rs) family. The MYB2Rs, with only two DNA-binding repeats, are not found in animals. In plants, they regulate diverse biological processes from development, metabolism, to response to environmental challenges (32). A second family of *Arabidopsis* MYB genes belong to the R1R2R3-MYBs (MYB3Rs) family. Only five MYB3Rs exist in *Arabidopsis*, which encode conserved cell cycle regulators found in animals (30–32). These five *Arabidopsis* MYB3Rs were shown to be either activators, MYB3R1 and MYB3R4, or repressors, MYB3R1, MYB3R3, and MYB3R5. The identification of only MYB3R1 and no other MYBs as the suppressor of *tso1-1* strongly suggests a unique role of MYB3R1 in cell cycle regulation and plant development.

The repressor MYB3R3 and activator MYB3R4 were found to associate with the repressor and activator DREAM complexes, respectively, in *Arabidopsis* seedlings (2, 4). While the repressor MYB3Rs were shown to promote cell cycle exit and organ differentiation, the activator MYB3Rs were responsible for activating the G2/M-specific gene expression, including the B1-type cyclin *CYCB1* and the plant-specific syntaxin *KNOLLE* (*KN*) for plant cell cytokinesis (2, 31, 33). Because of functional redundancy, none of the single mutants in the MYB3Rs showed any phenotypes (2, 31). Double mutants of activators *my3r1/4* showed a defect in mitosis and reduced expression of G2/M cell cycle genes in leaf stomata (33). In contrast, triple mutants of the repressor MYB3Rs, *myb3r1/3/5*, showed a constitutive expression of G2/M genes even outside cell cycle phase and ectopic cell division and overproliferation; the triple repressor mutants also showed significantly increased root meristem size, suggesting a delayed exit from cell proliferation (2). Kobayashi et al. (2) proposed that the activator MYB3Rs and

repressor MYB3Rs may work in different tissues and cell cycle phases, and they act in coordination rather than in competition. It is possible that MYB3R1 is critical to this coordination with its unique role both as an activator and a repressor in *Arabidopsis*.

***TSO1* and *MYB3R1* Form a Unique Partnership Regulating both the Shoot and Root.** In this study, 32 of the 45 suppressors of *tso1-1* cause loss-of-function mutations in the *MYB3R1* gene and none maps to the other four *MYB3Rs*, suggesting that *MYB3R1*, but not *MYB3R2*, *-3*, *-4*, and *-5*, is specifically regulated by *TSO1*. The ectopic and overexpression of *pMYB3R1::GUS* in the *tso1-1* mutant SAM and RAM suggests that wild-type *TSO1* is required to repress *MYB3R1* expression in the shoot and root. Since *myb3r1* loss-of-function mutations can suppress *tso1-1* phenotype in the SAM and RAM, the ectopic *MYB3R1* expression in *tso1-1* is necessary to mediate all aspects of the *tso1-1* mutant phenotypes. Our study functionally links TSO1 to MYB3R1 in plants and uncovers this critical TSO1-MYB3R1 module for proper shoot and root development.

Fig. 8 is a model that proposes how the TSO1-MYB3R1 regulatory module controls the cell cycle in the RAM and SAM. Among the five MYB3Rs, TSO1 likely represses *MYB3R1* only; the other four MYB3Rs are unlikely to be a target of *TSO1* or are minimally regulated by *TSO1*, as none of *tso1-1* suppressors maps to the other MYB3Rs. The effect of MYB3R1 as an activator ($MYB3R1^A$) in the shoot and a repressor ($MYB3R1^R$) in the root is also proposed. In the wild type, TSO1 represses the transcription of $MYB3R1^R$ so that cells can continuously proliferate in the root MZ (Fig. 8*A*). In *tso1-1* mutants, the ectopic expression of *MYB3R1* in the root MZ causes permanent cell cycle exit and premature differentiation, indicated by the root hair formation. However, in the SAM (Fig. 8*B*), TSO1 represses the $MYB3R1^A$ to prevent stem cells from entering the cell cycle. The repression of $MYB3R1^A$ by TSO1 mirrors the conserved function of the DREAM complex in repressing the B-MYB and other G1/S cell cycle genes in mammals (53, 54). In rapidly dividing cells such as those in floral primordia (Fig. 8*C*), TSO1 associates with the $MYB3R1^A$ to activate the G2/M cell cycle genes, just as their mammalian counterparts (LIN54 and B-MYB) do. This cooperation between TSO1 and the activator $MYB3R1^A$ provides an explanation for the incomplete cytokinesis phenotype found in the *tso1-1* SAM and *myb3r1/4* leaf stomata (17, 31) and is further supported by the co-IP data (Fig. 7).

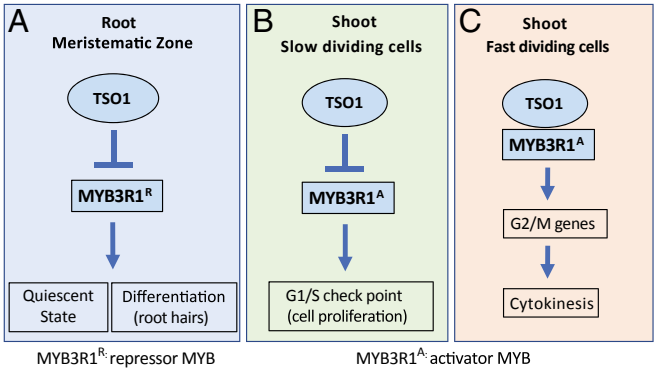

Fig. 8. A model of how the TSO1-MYB3R1 module balances cell proliferation with differentiation. TSO1 represses *MYB3R1* expression in both the root and the shoot. Arrows and bars indicate positive and negative regulations, respectively, by which they can be either direct or indirect. (*A*) In the root MZ, TSO1 represses the expression of the repressor $MYB3R1^R$ so that cells will not enter differentiation. In *tso1-1* mutants, ectopic expression of $MYB3R1^R$ in the root MZ causes cells to exit cell cycle and enter differentiation prematurely. (*B*) In the stem cells at the shoot apex, TSO1 represses the activator $MYB3R1^A$ to maintain a small pool of stem cells blocked at the G1/S checkpoint. (*C*) In rapidly proliferating floral primordia, TSO1 associates with the activator $MYB3R1^A$ to activate G2/M cell cycle genes, allowing smooth cell cycle progression and the completion of cytokinesis.

Our model provides a compelling explanation of why opposite effects were observed in the root and shoot of the *tso1-1* mutant, which had the ectopic expression and overexpression of *MYB3R1* in both the SAM and RAM. The overexpressed MYB3R1 in the SAM is an activator MYB, while the overexpressed MYB3R1 in the RAM acts as a repressor MYB. The suppression of the *tso1-1* phenotype suggests that the devastating effect of misregulated MYB3R1 can be reversed by removing the MYB3R1 through CRISPR. As the overexpression of B-MYB correlated with poor prognosis in numerous cancers (48, 49), removing the overexpressed B-MYB in cancer cells by RNAi or by CRISPR could reverse cancer progression, pointing to the B-MYB as a promising cancer treatment target. Furthermore, the genetic mosaic plant (Fig. 2*B*) reveals the cell-autonomous nature of the misexpressed MYB3R1 and informs about the somatic suppression vs. germline suppression, providing unprecedented insights into how the cell cycle abnormality is manifested in the context of a whole organism. Our work demonstrates the existence of a highly conserved TSO1/LIN54 to MYB3R1/B-MYB regulatory module in plants and animals, which plays a critical role in coordinating the cell cycle with the cell fate commitment.

Materials and Methods

Plant Materials and Growth Conditions. Plants were grown on Metromix soil (Griffin) under a 16-h light/8-h dark cycle at 20 °C. All mutants are in the Landsberg *erecta* (L*er*) background and were described previously: *tso1*-1 (17), *tso1-1*$^{+/+}$*sup-5* (28), and *tso1*-3 (29). The *tso1-3*$^{+/+}$*sup-5* heterozygous line was created by pollinating the *tso1-3* stigma with the *sup-5* (55) pollen. Genotyping derived cleaved amplified polymorphic sequence (dCAPs) markers for the *tso1* mutant alleles were described previously (28).

Vector Construction and Plant Transformation. All transformations were conducted using floral dip and *Agrobacterium* strain GV3101. Because of the *tso1-1* sterility, all constructs were transformed into tso1-1$^{+/+}$sup-5 or tso1-3$^{+/+}$sup-5 heterozygous plants. To construct *35S::TSO1-GR*, full-length *TSO1* cDNA was amplified from floral RNA with primers TSO1-GR.F and TSO1-GR.R (*SI Appendix*, Table S3) containing BamHI sites. The PCR fragment was inserted into *pBI121* (Clontech)-based *pBI-ΔGRBX* vector (56) at the BamHI site. One transgenic line homozygous for the *35S::TSO1-GR* transgene and *tso1-1* was selected for mutagenesis. Starting at the stage of bolting, DEX was sprayed daily to plant shoots for 10 d at 50-μM concentration (in water containing 0.015% Silwet L-77).

To generate *gTSO1*-GFP and translational fusion lines, a 4.1-kb *TSO1* genomic sequence containing a 1-kb promoter and full-length coding region (without the stop codon) was PCR amplified using Phusion (NEB) with primers TSO1.geno.F and TSO1.geno.R (*SI Appendix*, Table S3), and cloned into pCR8/GW/TOPO. After sequence confirmation, the genomic fragment was recombined into *pMDC107* (57) to create the *gTSO1-GFP*. T2 plants homozygous for *tso1-1* and the transgene were identified through PCR genotyping. Multiple transgenic lines showed the rescue of the mutant phenotype.

To generate *gTSO1-NLS-3xeGFP* with a stronger GFP signal, the 4.1-kb genomic fragment of *TSO1* was PCR amplified with primers p*TSO1*.F and *TSO1*0.3xGFP.n.R (*SI Appendix*, Table S3) to correct the reading frame and then recombined into *pGreenII-NLS-3xEGFP* (58).

The *pMYB3R1*::GUS reporter construct was generously provided by M. Ito, Nagoya University, Chikusa, Nagoya, Japan (31). Because of antibiotic selection incompatibility, the promoters from the above vector were cloned into *pMDC162* (57). The promoter was first PCR amplified from the above vector using Q5 (NEB) and cloned into pCR8/GW/TOPO, which was then LR recombined into the pMDC162 vector. Five T1 transgenic lines were characterized. T2 progeny from each of these five T1 plants were stained with X-Gluc based on a published protocol (59). The root tips were then incubated with clearing solution (8 g chloral hydrate: 1 mL 100% glycerol: 1 mL water) for 1 h and mounted on slides in clearing solution. To generate fluorescent transcriptional reporter, the *MYB3R1* promoter in the pCR8/GW/TOPO entry vector was recombined into *pGreenII-NLS-3xEGFP* (58).

To generate translational reporters for *MYB3R1*, a 6.4-kb genomic fragment containing the promoter and the gene body was PCR amplified using Q5 (NEB) with primers *pMYB3R1*.F and *MYB3R1*.non.stop.R (*SI Appendix*, Table S3) from L*er* wild-type DNA and cloned into pCR8/GW/TOPO. After sequence confirmation, the genomic fragment of *MYB3R1* was recombined into *pMDC107* (57) to create g*MYB3R1-GFP*. To generate a fluorescent

translational reporter line with a stronger GFP signal, the 6.4-kb genomic fragment of *MYB3R1* was PCR amplified with primers p*MYB3R1*.F and *MYB3R1*0.3xGFP.n.R (*SI Appendix*, Table S3) to correct the reading frame and recombined into *pGreenII-NLS-3xEGFP* (58).

To generate phosphomimic *gMYB3R1-GFP* constructs, the pCR8/GW/TOPO vector harboring the 6.4-kb *MYB3R1* genomic fragment was modified using the Q5 Site-Directed Mutagenesis KIT (NEB) following the manufacturer's instruction. Briefly, primers S656D.F/S656D.R (*SI Appendix*, Table S3) were used to amplify the *MYB3R1* 6.4-kb gDNA TOPO construct. The changes in the coding sequence resulted in the change of 656 serine to aspartic acid (S656D). Similarly, primers S709D.F/S709D.R (*SI Appendix*, Table S3) were used to generate the S709D. The modified *MYB3R1* gDNA pCR8/GW/TOPO constructs were recombined into *pMDC107* (57) to generate g*MYB3R1* (*S656D*) and g*MYB3R1* (*S709D*), respectively.

To generate constructs for co-IP assay, the *TSO1* cDNA was cloned into *PHB-FLAG-X* vector (60) to generate 35S::Flag-TSO1. The *35S::MYB3R1* (cDNA) construct was generously provided by M. Ito (30). The cDNA was PCR amplified using MYB3R1.F and MYB3R1.R (*SI Appendix*, Table S3) and then subcloned into pEarleyGate104 (61) to generate *35S::YFP-MYB3R1*. The cDNA was also recombined into pEarleyGate100 (61) to generate *35S::MYB3R1*.

Suppressor Screen and Complementation Tests. The genetic screen scheme is shown in *SI Appendix*, Fig. S1. *35S::TSO1-GR*; *tso1-1* homozygous seeds were treated with 0.2% EMS solution for 12 h. After repeatedly washing off the mutagen with water, the seeds were germinated in soil and M1 plant fertility was restored by DEX spray. For the first 2,000 M1 plants, seeds were collected from individual M1 plants. For the next 1,000 M1 plants, seeds were pooled into one pool. M2 plants were screened for the ability to form elongated siliques. Forty-five suppressors were identified from screening the progeny of ∼3,000 M1 plants. These M2 suppressor plants were backcrossed to the parental line *35S::TSO1-GR; tso1-1* to generate the mapping population. For each suppressor, the F1 progeny at bolting was supplied with DEX to allow for seed production. The resulting F2 progeny showed suppressed (∼25%) and unsuppressed (∼75%) phenotype; these two populations served as the mapping populations (*SI Appendix*, Fig. S1).

For complementation test, M2 suppressor lines were crossed with one another. Since the suppressors are recessive, F1 progeny should show unsuppressed phenotype unless the suppressor mutations are allelic to each other, which would show suppressed phenotype in F1.

Mapping by Sequencing. For each suppressor F2 mapping population, leaf tissues were collected and pooled from 35–50 plants, and genomic DNA was extracted from the pooled leaf tissue using the NucleoSpin Plant II Midi Kit (Macherey-Nagel). Each DNA pool was sequenced at 15–20× coverage with 51-bp single end reads (*SI Appendix*, Table S4). Reads were aligned to the TAIR10 *Arabidopsis* genome with Bowtie2 (62) and variants were called with SAMtools (63). Six independent suppressors (A144, A156, A176, A317, B636, and B763) were mapped and sequenced. A *35S::TSO1-GR*; *tso1-1* parental line was also sequenced at about 8× coverage (*SI Appendix*, Table S4). Variants shared among all six samples (556,864 total variants) are likely carried over from prior EMS mutagenesis that generated *tso1-1* in the L*er* background. They were removed from further analysis. SNPs unique to each suppressor pool were identified using the genotype calling feature of SAMtools (64). G-to-A or C-to-T changes were further selected as candidate SNPs as they are most likely caused by EMS. The enrichment of candidate SNPs in 100,000-bp window was plotted using R (*SI Appendix*, Fig. S3). Annotation of variants was done using the VariantAnnotation package (65) from Bioconductor to identify nonsynonymous SNPs within exons as well as SNPs affecting splicing.

CRISPR/Cas9 Gene Editing and Genotyping of the Resulting Mutants. gRNA was designed using crispr.dbcls.jp/. The 20-bp seed RNA targets the fourth exon of *MYB3R1* coding for a region between R1 and R2 of MYB3R1. Blast search against the *Arabidopsis* genome did not identify any other target homology. The target RNA sequence (ACGGTCCTTTCACAAGCTCT) was inserted between the *AtU6* promoter and scaffold followed by the *AtU6* terminator using overlapping PCR (*SI Appendix*, Table S3) with pCAMBIA-Cas9+gRNA (66) as the template. The above PCR fragment was cloned into pCR8/GW/TOPO, excised by SalI and KpnI, and ligated into SalI and KpnI sites in pCAMBIA-Cas9+sgRNA (66). T1 seeds were screened on 1/2 MS medium containing hygromycin. T2 plants showing chimeric wild-type branches in *tso1-1* homozygous plants were further analyzed. DNA was extracted from the individual suppressed branches, and PCR primers (MYB3R1.CRISPR.con.F/R; *SI Appendix*, Table S3) were used to amplify DNA fragments spanning the gRNA target site within *MYB3R1*, which were then sequenced. For *tso1-3*$^{+/+}$ *sup-5* plants transformed with the CRISPR constructs, DNA was extracted from six T2 plants showing slightly improved fertility and sequenced to reveal heterozygous mutations in *MYB3R1*. T3 progeny of these six T2 plants segregated 25% of completely rescued plants.

To construct CRISPR vector for *MYB3R4* gene editing, gRNA was designed to target the second exon. Primers MYB3R4.CRIPSR.F/R (*SI Appendix*, Table S3) were annealed and ligated into the BsaI cutting site of the pHEE401E vector (67). The construct was introduced into *tso1-1*$^{+/+}$*sup-5* plants. CRISPR-generated mutations likely destroy a BbvCI restriction site at the gRNA target, allowing rapid screening of CRISPR-induced mutations. PCR primers MYB3R4.seq.pro.F and MYB3R4.fourth.exon.R (*SI Appendix*, Table S3) amplified the DNA fragment spanning the gRNA target site for sequencing.

Confocal Microscopy and Data Processing. For RAM imaging, 7-d-old seedlings were immersed in 10 μg/mL PI in water for 2 min. The roots were then mounted on slides in water and observed using the 63× (1.2 HCXPLAPO CS) water objective of a Leica SPX5 confocal microscope. A fluorescent signal, excited by a white light laser at 536 nm, was detected with detection channel set at 550 nm–660 nm. Tile scans were taken and processed using Leica Application Suite 2.0.0 software.

For SAM imaging, inflorescences from 4-wk-old plants were dissected to remove flowers older than stage 5 (68). The inflorescence apexes were stained with 10 μg/mL PI for 3–5 min and mounted in a Nunc Lab-Tek chamber slide. Z stacks of PI (600–650 nm) and GFP (500–545 nm) channels were acquired with 63× (1.2 HCXPLAPO CS) water objective of a Leica SPX5 inverted confocal microscope. Scanning speed was set at 400 Hz to achieve 0.48 × 0.48 × 0.46 μm voxel size. Fiji (fiji.sc/) was used to extract .tiff files. The 3D segmentation of cells and flourescent signal heatmap were generated following instructions from LithoGraphX website section 4.3, Segmenting Cells in 3D (lithographx.org) (69).

Fertility Quantification and qRT-PCR Analysis of Transgenic Plants. For fertility quantification (*SI Appendix*, Fig. S6*B*), siliques in the 5th–15th positions from the base were collected. Seeds per silique were quantified. The main shoots of 5–10 plants per transgenic line were quantified. For qRT-PCR (*SI Appendix*, Fig. S6*C*), inflorescence containing unopened flowers was collected for RNA extraction using TRIzol reagent (Ambion no. 66316). A total of 1 μg RNA from each sample was treated with RNase-Free DNase I (Thermo Scientific, no. EN0521) followed by first strand cDNA synthesis using the RevertAid First Strand cDNA Synthesis Kit (Thermo Scientific, no. K1621). Real-time quantitative PCR was performed using SsoFast EvaGreen supermix (Bio-Rad). Since the *gMYB3R1* transgene is tagged by GFP, a reverse PCR primer against GFP (*SI Appendix*, Table S3) was used to distinguish the transgene from the endogenous *MYB3R1* gene. Three biological replicates, each with three technical replicates, were performed for each transgenic line.

Coimmunoprecipitation Assays. The *Agrobacterium* harboring *35S::Flag-TSO1* and *35S::YFP-MYB3R1* were used to cotransfect tobacco leaves by infiltration. Samples were collected after 48 h and ground in liquid nitrogen and homogenized in the lysis buffer (50 mM Tris·HCl pH7.5, 150 mM NaCl, 1 mM EDTA, 10% glycerol, 0.2% Triton-X-100, 1 mM Pefabloc, mixture, 50 μM MG132). After centrifugation, supernatant was incubated with 1 μL anti-Flag (Sigma) antibody [or with 5 μL anti-GFP (cat. no. A01388-100, rabbit; GenScript)] bound to 10 μL protein G (Invitrogen) beads for 2 h at 4 °C. Then the beads were washed three times with 1 mL of the lysis buffer and eluted by boiling with 20 μL 2× SDS sample buffer for 5 min and then separated on 10% SDS/PAGE gel. Anti-Flag (Sigma; 1:5,000) and anti-GFP (TransGen Biotech; 1:2,000) antibodies were used to detect Flag-TSO1 and YFP-MYB3R1, respectively.

ACKNOWLEDGMENTS. We thank Drs. Masaki Ito, Qi-Jun Chen, and Donald Weeks for providing *MYB3R1::GUS*, *35S::MYB3R1*, and *CRISPR* constructs; the undergraduate students who contributed to this project; Michael Wellen and Rao Fu for helping with seed collection at the early stage of the genetic screen; Dae Ik Yi, Xixi Zhou, and Song Yun for making constructs and assisting in transformation; Dr. Chunying Kang for comments on the manuscript; and Amy Beaven and the Department of Cell Biology and Molecular Genetics Imaging Core for assistance with confocal fluorescence microscopy. The work was supported by National Science Foundation Grant MCB0951460 (to Z.L.), and China Scholarship Council Postgraduate Scholarship (to W.W.).

1. Inzé D, De Veylder L (2006) Cell cycle regulation in plant development. *Annu Rev Genet* 40:77–105.
2. Kobayashi K, et al. (2015) Transcriptional repression by MYB3R proteins regulates plant organ growth. *EMBO J* 34:1992–2007.
3. Sadasivam S, DeCaprio JA (2013) The DREAM complex: Master coordinator of cell cycle-dependent gene expression. *Nat Rev Cancer* 13:585–595.
4. Fischer M, DeCaprio JA (2015) Does Arabidopsis thaliana DREAM of cell cycle control? *EMBO J* 34:1987–1989.
5. Paulovich AG, Toczyski DP, Hartwell LH (1997) When checkpoints fail. *Cell* 88:315–321.
6. Litovchick L, et al. (2007) Evolutionarily conserved multisubunit RBL2/p130 and E2F4 protein complex represses human cell cycle-dependent genes in quiescence. *Mol Cell* 26:539–551.
7. Pfeiffer A, Wenzl C, Lohmann JU (2017) Beyond flexibility: Controlling stem cells in an ever changing environment. *Curr Opin Plant Biol* 35:117–123.
8. Petricka JJ, Winter CM, Benfey PN (2012) Control of Arabidopsis root development. *Annu Rev Plant Biol* 63:563–590.
9. Sarkar AK, et al. (2007) Conserved factors regulate signalling in Arabidopsis thaliana shoot and root stem cell organizers. *Nature* 446:811–814.
10. Weinberg RA (1995) The retinoblastoma protein and cell cycle control. *Cell* 81: 323–330.
11. Friend SH, et al. (1986) A human DNA segment with properties of the gene that predisposes to retinoblastoma and osteosarcoma. *Nature* 323:643–646.
12. Jacks T, et al. (1992) Effects of an Rb mutation in the mouse. *Nature* 359:295–300.
13. Ebel C, Mariconti L, Gruissem W (2004) Plant retinoblastoma homologues control nuclear proliferation in the female gametophyte. *Nature* 429:776–780.
14. Johnston AJ, Matveeva E, Kirioukhova O, Grossniklaus U, Gruissem W (2008) A dynamic reciprocal RBR-PRC2 regulatory circuit controls Arabidopsis gametophyte development. *Curr Biol* 18:1680–1686.
15. Johnston AJ, Gruissem W (2009) Gametophyte differentiation and imprinting control in plants: Crosstalk between RBR and chromatin. *Commun Integr Biol* 2:144–146.
16. Borghi L, et al. (2010) Arabidopsis RETINOBLASTOMA-RELATED is required for stem cell maintenance, cell differentiation, and lateral organ production. *Plant Cell* 22: 1792–1811.
17. Liu Z, Running MP, Meyerowitz EM (1997) TSO1 functions in cell division during Arabidopsis flower development. *Development* 124:665–672.
18. Song JY, Leung T, Ehler LK, Wang C, Liu Z (2000) Regulation of meristem organization and cell division by TSO1, an Arabidopsis gene with cysteine-rich repeats. *Development* 127:2207–2217.
19. Hauser BA, He JQ, Park SO, Gasser CS (2000) TSO1 is a novel protein that modulates cytokinesis and cell expansion in Arabidopsis. *Development* 127:2219–2226.
20. Beall EL, et al. (2002) Role for a Drosophila Myb-containing protein complex in site-specific DNA replication. *Nature* 420:833–837.
21. Beall EL, et al. (2007) Discovery of tMAC: A Drosophila testis-specific meiotic arrest complex paralogous to Myb-Muv B. *Genes Dev* 21:904–919.
22. Harrison MM, Ceol CJ, Lu X, Horvitz HR (2006) Some C. elegans class B synthetic multivulva proteins encode a conserved LIN-35 Rb-containing complex distinct from a NuRD-like complex. *Proc Natl Acad Sci USA* 103:16782–16787.
23. Jiang J, Benson E, Bausek N, Doggett K, White-Cooper H (2007) Tombola, a tesmin/TSO1-family protein, regulates transcriptional activation in the Drosophila male germline and physically interacts with always early. *Development* 134:1549–1559.
24. Schmit F, et al. (2007) LINC, a human complex that is related to pRB-containing complexes in invertebrates regulates the expression of G2/M genes. *Cell Cycle* 6: 1903–1913.
25. Korenjak M, et al. (2004) Native E2F/RBF complexes contain Myb-interacting proteins and repress transcription of developmentally controlled E2F target genes. *Cell* 119: 181–193.
26. Lewis PW, et al. (2004) Identification of a Drosophila Myb-E2F2/RBF transcriptional repressor complex. *Genes Dev* 18:2929–2940.
27. Andersen SU, et al. (2007) The conserved cysteine-rich domain of a tesmin/TSO1-like protein binds zinc in vitro and TSO1 is required for both male and female fertility in Arabidopsis thaliana. *J Exp Bot* 58:3657–3670.
28. Sijacic P, Wang W, Liu Z (2011) Recessive antimorphic alleles overcome functionally redundant loci to reveal TSO1 function in Arabidopsis flowers and meristems. *PLoS Genet* 7:e1002352.
29. Hauser BA, Villanueva JM, Gasser CS (1998) Arabidopsis TSO1 regulates directional processes in cells during floral organogenesis. *Genetics* 150:411–423.
30. Ito M (2005) Conservation and diversification of three-repeat Myb transcription factors in plants. *J Plant Res* 118:61–69.
31. Haga N, et al. (2007) R1R2R3-Myb proteins positively regulate cytokinesis through activation of KNOLLE transcription in Arabidopsis thaliana. *Development* 134: 1101–1110.
32. Dubos C, et al. (2010) MYB transcription factors in Arabidopsis. *Trends Plant Sci* 15: 573–581.
33. Haga N, et al. (2011) Mutations in MYB3R1 and MYB3R4 cause pleiotropic developmental defects and preferential down-regulation of multiple G2/M-specific genes in Arabidopsis. *Plant Physiol* 157:706–717.
34. Wang C, Liu Z (2006) Arabidopsis ribonucleotide reductases are critical for cell cycle progression, DNA damage repair, and plant development. *Plant Cell* 18:350–365.
35. Dello Ioio R, et al. (2008) A genetic framework for the control of cell division and differentiation in the root meristem. *Science* 322:1380–1384.
36. Perilli S, Sabatini S (2010) Analysis of root meristem size development. *Methods Mol Biol* 655:177–187.
37. Brady SM, et al. (2007) A high-resolution root spatiotemporal map reveals dominant expression patterns. *Science* 318:801–806.
38. Sala A, et al. (1997) Activation of human B-MYB by cyclins. *Proc Natl Acad Sci USA* 94: 532–536.
39. Johnson TK, Schweppe RE, Septer J, Lewis RE (1999) Phosphorylation of B-Myb regulates its transactivation potential and DNA binding. *J Biol Chem* 274:36741–36749.
40. Heazlewood JL, et al. (2008) PhosPhAt: A database of phosphorylation sites in Arabidopsis thaliana and a plant-specific phosphorylation site predictor. *Nucleic Acids Res* 36: D1015–D1021.
41. Durek P, et al. (2010) PhosPhAt: The Arabidopsis thaliana phosphorylation site database. An update. *Nucleic Acids Res* 38:D828–D834.
42. Umezawa T, et al. (2013) Genetics and phosphoproteomics reveal a protein phosphorylation network in the abscisic acid signaling pathway in Arabidopsis thaliana. *Sci Signal* 6:rs8.
43. Wang X, et al. (2013) A large-scale protein phosphorylation analysis reveals novel phosphorylation motifs and phosphoregulatory networks in Arabidopsis. *J Proteomics* 78:486–498.
44. Schmit F, Cremer S, Gaubatz S (2009) LIN54 is an essential core subunit of the DREAM/LINC complex that binds to the cdc2 promoter in a sequence-specific manner. *FEBS J* 276:5703–5716.
45. Kittler R, et al. (2007) Genome-scale RNAi profiling of cell division in human tissue culture cells. *Nat Cell Biol* 9:1401–1412.
46. Matsuo T, Kuramoto H, Kumazaki T, Mitsui Y, Takahashi T (2012) LIN54 harboring a mutation in CHC domain is localized to the cytoplasm and inhibits cell cycle progression. *Cell Cycle* 11:3227–3236.
47. Beall EL, Bell M, Georlette D, Botchan MR (2004) Dm-myb mutant lethality in Drosophila is dependent upon mip130: Positive and negative regulation of DNA replication. *Genes Dev* 18:1667–1680.
48. Musa J, Aynaud M-M, Mirabeau O, Delattre O, Grünewald TG (2017) MYBL2 (B-Myb): A central regulator of cell proliferation, cell survival and differentiation involved in tumorigenesis. *Cell Death Dis* 8:e2895.
49. Amatschek S, et al. (2004) Tissue-wide expression profiling using cDNA subtraction and microarrays to identify tumor-specific genes. *Cancer Res* 64:844–856.
50. Heine GF, Hernandez JM, Grotewold E (2004) Two cysteines in plant R2R3 MYB domains participate in REDOX-dependent DNA binding. *J Biol Chem* 279:37878–37885.
51. Grässer FA, LaMontagne K, Whittaker L, Stohr S, Lipsick JS (1992) A highly conserved cysteine in the v-Myb DNA-binding domain is essential for transformation and transcriptional trans-activation. *Oncogene* 7:1005–1009.
52. Guehmann S, Vorbrueggen G, Kalkbrenner F, Moelling K (1992) Reduction of a conserved Cys is essential for Myb DNA-binding. *Nucleic Acids Res* 20:2279–2286.
53. Fischer M, Grossmann P, Padi M, DeCaprio JA (2016) Integration of TP53, DREAM, MMB-FOXM1 and RB-E2F target gene analyses identifies cell cycle gene regulatory networks. *Nucleic Acids Res* 44:6070–6086.
54. Fischer M, Müller GA (2017) Cell cycle transcription control: DREAM/MuvB and RB-E2F complexes. *Crit Rev Biochem Mol Biol* 52:638–662.
55. Gaiser JC, Robinson-Beers K, Gasser CS (1995) The Arabidopsis SUPERMAN gene mediates asymmetric growth of the outer integument of ovules. *Plant Cell* 7:333–345.
56. Lloyd AM, Schena M, Walbot V, Davis RW (1994) Epidermal cell fate determination in Arabidopsis: Patterns defined by a steroid-inducible regulator. *Science* 266:436–439.
57. Curtis MD, Grossniklaus U (2003) A gateway cloning vector set for high-throughput functional analysis of genes in planta. *Plant Physiol* 133:462–469.
58. Takada S, Jürgens G (2007) Transcriptional regulation of epidermal cell fate in the Arabidopsis embryo. *Development* 134:1141–1150.
59. Takahashi N, et al. (2013) Cytokinins control endocycle onset by promoting the expression of an APC/C activator in Arabidopsis roots. *Curr Biol* 23:1812–1817.
60. Luo Q, et al. (2014) COP1 and phyB physically interact with PIL1 to regulate its stability and photomorphogenic development in Arabidopsis. *Plant Cell* 26:2441–2456.
61. Earley KW, et al. (2006) Gateway-compatible vectors for plant functional genomics and proteomics. *Plant J* 45:616–629.
62. Langmead B, Salzberg SL (2012) Fast gapped-read alignment with Bowtie 2. *Nat Methods* 9:357–359.
63. Li H, et al.; 1000 Genome Project Data Processing Subgroup (2009) The sequence alignment/map format and SAMtools. *Bioinformatics* 25:2078–2079.
64. Li H (2011) A statistical framework for SNP calling, mutation discovery, association mapping and population genetical parameter estimation from sequencing data. *Bioinformatics* 27:2987–2993.
65. Obenchain V, et al. (2014) VariantAnnotation: A bioconductor package for exploration and annotation of genetic variants. *Bioinformatics* 30:2076–2078.
66. Jiang W, Yang B, Weeks DP (2014) Efficient CRISPR/Cas9-mediated gene editing in Arabidopsis thaliana and inheritance of modified genes in the T2 and T3 generations. *PLoS One* 9:e99225.
67. Wang Z-P, et al. (2015) Egg cell-specific promoter-controlled CRISPR/Cas9 efficiently generates homozygous mutants for multiple target genes in Arabidopsis in a single generation. *Genome Biol* 16:144.
68. Smyth DR, Bowman JL, Meyerowitz EM (1990) Early flower development in Arabidopsis. *Plant Cell* 2:755–767.
69. Barbier de Reuille P, et al. (2015) MorphoGraphX: A platform for quantifying morphogenesis in 4D. *eLife* 4:05864.